*Materials Research*. 2023; 26(suppl. 1): e20220534
DOI: https://doi.org/10.1590/1980-5373-MR-2022-0534

# Wave Attenuation in 1-D Viscoelastic Phononic Crystal Rods Using Different Polymers

***Vinícius Braga Santos de Oliveira*[a], *Lucas Franco Corrêa Schalcher*[b],**

***José Maria Campos Dos Santos*[c], *Edson Jansen Pedrosa de Miranda Jr.*[b,d]***

[a]*Instituto Federal do Maranhão (IFMA), Departamento de Mecânica e Materiais (DMM), Avenida Getúlio Vargas, 4, CEP 65030-005, São Luís, MA, Brasil.*
[b]*Instituto Federal do Maranhão (IFMA), Programa de Pós-Graduação em Engenharia de Materiais (PPGEM), Avenida Getúlio Vargas, 4, CEP 65030-005, São Luís, MA, Brasil.*
[c]*Universidade Estadual de Campinas (UNICAMP), Faculdade de Engenharia Mecânica (FEM), Departamento de Mecânica Computacional (DMC), Rua Mendeleyev, 200, CEP 13083-970, Campinas, SP, Brasil.*
[d]*Instituto Federal do Maranhão (IFMA), Extensão Itaqui Bacanga (EIB), Departamento de Ensino (DE), Rua Afonso Pena, 174, CEP 65010-030, São Luís, MA, Brasil.*

Received: December 10, 2022; Revised: March 16, 2023; Accepted: April 26, 2023

The elastic wave attenuation in artificial composites, known as phononic crystals (PnCs), is an important topic in the context of wave manipulation. However, there is a lack of knowledge in the obtainment of the wave attenuation of PnCs when the viscoelastic effect of different polymers is considered. In this study, the complex band structure of longitudinal waves in 1-D viscoelastic PnC (VPnC) rods composed by steel inclusions (elastic material) in a polymeric matrix (viscoelastic material) is investigated. The viscoelastic effect is modelled by the standard linear solid model (SLSM), which can be used to closely model the behavior of polymers for practical applications. It is also studied the influence of different polymers (i.e., epoxy, nylon, silicon rubber, natural rubber, and low density polyethylene (LDPE)) on the complex band structure of 1-D VPnC rods. The improved plane wave expansion (IPWE) and extended plane wave expansion (EPWE) are used to compute the band structure. It is observed that the viscoelastic effect influences significantly both the propagating and evanescent waves. The viscoelasticity increases the unit cell wave attenuation for most range of frequency considering all polymeric matrices. The highest unit cell wave attenuation is for the polymeric matrix of natural rubber.

**Keywords:** *Periodic structures, complex band structure, viscoelasticity, band gaps, vibration attenuation.*

## 1. Introduction

Artificial composites, known as phononic crystals (PnCs) and/or mechanical metamaterials, are structures designed to achieve unusual properties and applications, such as vibration control[1,2], acoustic barriers[3,4], wave manipulation (e.g., guiding, focusing, imaging, cloaking, and topological insulation)[5,6], energy harvesting[7], and negative Poisson's ratio[8]. They are typically composed by periodic arrays of inclusions embedded in a matrix[9,10] to open up band gaps arising from Bragg scattering and/or local resonance[11]. In these forbidden ranges of frequency (i.e., band gaps), there are only evanescent Bloch waves[12] and waves cannot propagate.

The viscoelastic effect in most cases is neglected considering the wave propagation in PnCs[12-14]. However, more recently, this effect is being studied for the viscoelastic phononic crystals (VPnCs)[11,15-22]. Vakilifard and Mahmoodi[16] investigated the complex band structure, wave transmission spectra, and effective stiffness of a carbon nanotube- modified viscoelastic locally resonant metamaterial (LRM). They[16] observed that this nano LRM exhibits simultaneously higher stiffness and loss factor with respect to ordinary LRMs. Moreover, they[16] also reported that the volume fraction and aspect ratio have the most influential effects on the nano LRM properties. Chen et al.[19] noted that the viscoelasticity of constituent materials has a significant effect on the band structure of the VPnCs. They[19] found novel topological patterns of the optimized VPnCs by using the bi-directional evolutionary structure optimization (BESO) method. Dal Poggetto and collaborators[11] studied the complex band structure of hierarchical VPnC thick plates. They[11] mentioned that an increase in the hierarchical order leads to a weight reduction with relatively preserved attenuation characteristics (for the case of a hard purely elastic matrix with soft viscoelastic inclusions). They[11] also reported that changing the hierarchical order implies in opening band gaps in distinct frequency ranges, with an overall attenuation improved by an increase in the viscoelasticity (for the case of soft viscoelastic matrix with hard purely elastic inclusions).

The majority of the studies about wave propagation in VPnCs considered simple models of viscosity, for instance, the Kelvin-Voigt model (consists of a spring and dashpot in parallel[23], i.e., the viscosity is proportional to the frequency). However, the simpler the model is, the more difficult it is to be applied to simulate the behavior of a viscoelastic material.

*e-mail: edson.jansen@ifma.edu.br

On this account, the standard linear solid model (SLSM) is considered in this study, which contains three elements, i.e., a Maxwell model (a spring and dashpot in series) and a spring in parallel[23]. The SLSM is one of the most common and popular viscoelastic models used to describe and analyse viscoelastic behaviors of viscoelastic solids[24]. It can be used to simulate viscoelastic behaviors for understanding rich phenomena and underlying mechanisms of viscoelasticicity[24]. The SLSM has several advantages, for instance, it has only three elements, therefore its analysis results are much easier to be interpreted compared to those using models having a large number of elements (such as the generalized Maxwell and Kelvin models)[24].

Another interesting and necessary aspect in terms of wave propagation in VPnCs is to consider the presence of evanescent waves in the band structure (i.e., the complex band structure) calculation[25]. Recently, some strategies of increasing wave attenuation have been proposed by maximizing spatial decay of evanescent waves, for example by topology optimization[19], multiple periodic resonators[12], coupling local resonance and Bragg band gaps[12], and using hierarchical periodic structures[11]. Very recently, Schalcher et al.[26] formulated the extended plane wave expansion (EPWE) to handle 1-D VPnC solids (i.e., plane strain condition) modelled by the SLSM to obtain the complex band structure. However, they[26] considered just one type of polymer, i.e., epoxy as the viscoelastic matrix, and bulk wave propagation (i.e., the 1-D VPnC solid has infinite thickness and height).

To the best of our knowledge, this is the first study to investigate the complex band structure of longitudinal waves in 1-D VPnC rods with different polymers considering the SLSM. In this context, the main purpose of this investigation is to analyze the complex band structure of 1-D VPnC rods composed by steel inclusions in a polymeric matrix considering the viscoelastic effect modelled by the SLSM. The influence of different materials for the polymeric matrix (i.e., epoxy, nylon, silicon rubber, natural rubber, and low density polyethylene (LDPE)) on the band gap behavior and wave attenuation is analyzed. The improved plane wave expansion (IPWE), $\omega(\mathrm{k})$ approach[27,28], and the EPWE, $\mathrm{k}(\omega)$ approach[29,30], are used to calculate the band structure of the VPnC rod, where $\omega$ is the angular frequency and $\mathrm{k}$ is the wave number.

The paper is organized as follows. Section 2 presents details for the 1-D VPnC rod modelling. In Section 3, simulated examples are carried out. Conclusions are presented in Section 4.

## 2. 1-D Viscoelastic Phononic Crystal Rod Modelling

Figure 1 sketches the front view of the 1-D VPnC rod with steel inclusions (white) distributed in a polymeric matrix (i.e., epoxy, nylon, silicon rubber, natural rubber, or LDPE) (blue) ($a$), where $a$ is the unit cell length, and the SLSM[23] (b). The first Brillouin zone (FBZ)[31] for the 1-D case is $-\pi/\mathrm{a} \le \mathrm{k} \le \pi/\mathrm{a}$. The SLSM is used to consider the viscoelasticity of the polymeric matrix, where $G_1$ and $G_2$ are the shear modulus (springs), and $\eta$ is the viscosity (dashpot)[23] in Figure 1b. It is important to mention that the inclusions and matrix are considered as isotropic materials in this study.

For the modelling, IPWE and EPWE approaches are used to calculate the band structure (only propagating waves) and complex band structure (both propagating and evanescent waves), respectively. IPWE and EPWE formulations are similar to those derived for 1-D PnCs[32]. However, those formulations[32] can handle only the case of 1-D PnCs without viscoelastic effect.

The EPWE approach is important to obtain the information of wave attenuation of the unit cell (i.e., $\Im\{\mathrm{k}\}\mathrm{a}$ [12]). Moreover, by using EPWE, one can calculate the purely imaginary and complex values of $\mathrm{k}$ (i.e., evanescent wave modes) that cannot be directly computed by the PWE. Thus, the use of EPWE method is necessary for damped structures and VPnCs, since all wave modes become evanescent.

In order to include the viscoelasticity, the elastic constants in the study of Assis et al.[32], considering the polymeric matrix, should be calculated following the Equation 1[23,26]:

$$G(t) = \left[ G_\infty + (G_0 + G_\infty) e^{-\frac{t}{\tau_G}} \right] u(t), \tag{1}$$

where u(t) is the unit step function, t is the time, $\tau_G$ is the relaxation time, $G_0$ and $G_\infty$ are the initial and final states of the elastic constants, and they are related to $G_1$ and $G_2$ (see Figure 1b) as $G_\infty = G_2$ and $G_1 = G_0 - G_\infty$. Applying the temporal Fourier transform to Equation 1, results in[26]:

$$\mathrm{G}(\omega) = \frac{(\mathrm{G}_0 - \mathrm{G}_\infty)\tau_\mathrm{G}}{1+\omega^2\tau_\mathrm{G}^2} - i\frac{\mathrm{G}_\infty + \mathrm{G}_0\omega^2\tau_\mathrm{G}^2}{\omega\left(1+\omega^2\tau_\mathrm{G}^2\right)}, \tag{2}$$

where i is the unit imaginary number.

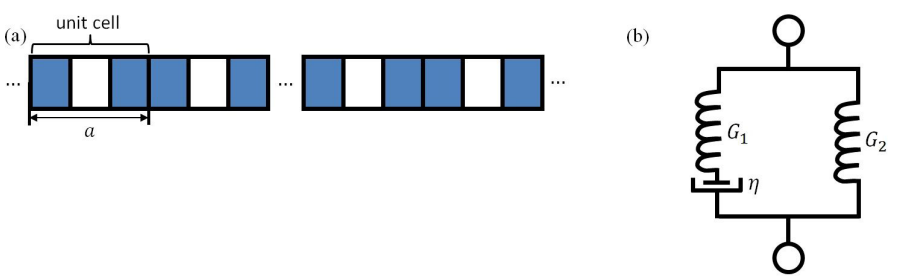


**Figure 1.** Front view of the 1-D VPnC rod with steel inclusions (white) in a polymeric matrix (*i.e.*, epoxy, nylon, silicon rubber, natural rubber, or LDPE) (blue) (a), where $a$ is the unit cell length, and the SLSM (b), where $G_1$ and $G_2$ are the shear modulus (springs), and $\eta$ is the viscosity (dashpot) (b).

It should be highlighted that IPWE method has higher convergence than the traditional plane wave expansion (PWE) method[27,28]. Moreover, the band structure computed by IPWE shows a considerably lower computational cost[11], since it is a semi-analytical approach and it is not necessary to consider a large number of degrees-of-freedom (DOFs) as with finite element (FE)[33] for instance.

## 3. Simulated Examples

The properties of the 1-D VPnC rod composed by steel inclusions (A) and polymeric matrix (i.e., epoxy, nylon, silicon rubber, natural rubber, or LDPE) (B) used for the simulation[34-39] are listed in Table 1. Moreover, the viscoelastic effect is considered with the following properties[35] $\tau_G = 1\times10^{-4}$ s and $G_{\infty_B} = G_{0_B}/5$ from now on.

Hereafter, the model assurance criterion (MAC)[40] is used to estimate the correlation among wave mode shapes for EPWE. Furthermore, initially, for band structure and complex band structure calculation using IPWE and EPWE, respectively, it is considered 21 plane waves. In order to verify the convergence of IPWE, the band structure (only propagating waves) of the 1-D VPnC rod with steel inclusions in a polymeric matrix (i.e., (a) epoxy, (b) nylon, (c) LDPE, (d) natural rubber, and (e) silicon rubber) without viscoelasticity was computed (Figure 2) considering 21 (black circles) and 42 (red points) plane waves, where $c_L = \sqrt{G_{0_B}/\rho_B}$ is the longitudinal wave velocity in the matrix. It can be observed a good agreement between the wave modes. However, a considerable mismatching can be observed near $\omega a/2\pi c_L > 6$. Even so, 21 plane waves are regarded in order to reduce the computational time.

In Figure 3, it is shown the complex band structure of the 1-D VPnC rod without (a-b) and with (c-d) viscoelasticity considering epoxy as the polymeric matrix computed by IPWE (black circles in (a, c)) and EPWE (colored points in (a-d)) approaches.

**Table 1.** Geometry and material properties of the 1-D VPnC rod composed by steel inclusions (A)[34] in a polymeric matrix (*i.e.*, epoxy[35,36], nylon[37], silicon rubber[38], natural rubber[38] or LDPE[39]) (B).

| Geometry/Property | Value |
|---|---|
| Lattice parameter $(a)$ | 40 m |
| Rod thickness $(h)$ | 10 m |
| Rod height ($b$) | 10 m |
| Filling fraction $(\bar{f})$ | 0.5 |
| Mass density $\left(\rho_A, \rho_{B(epoxy)}\right)$ | 7835 kg/m$^3$, 1180 kg/m$^3$ |
| Young's modulus $\left(E_A, E_{0_{B(epoxy)}}\right)$ | 210.3 x 10$^9$ Pa, 3.491 x 10$^9$ Pa |
| Shear modulus $\left(G_A, G_{0_{B(epoxy)}}\right)$ | 81.65 x 10$^9$ Pa, 1.58 x 10$^9$ Pa |
| Poisson's ratio $\left(\nu_A, \nu_{B(epoxy)}\right)$ | 0.2878, 0.105 |
| Young's modulus $\left(E_{0_{B(nylon)}}, E_{0_{B(silicon)}}\right)$ | 1 x 10$^9$ Pa, 0.001 x 10$^9$ Pa |
| Shear modulus $\left(G_{0_{B(nylon)}}, G_{0_{B(silicon)}}\right)$ | 3.571 x 10$^8$ Pa, 3.401 x 10$^5$ Pa |
| Poisson's ratio $\left(\nu_{0_{B(nylon)}}, \nu_{0_{B(silicon)}}\right)$ | 0.4, 0.47 |
| Young's modulus $\left(E_{0_{B(natural)}}, E_{0_{B(LDPE)}}\right)$ | 0.01 x 10$^9$ Pa, 0.1 x 10$^9$ Pa |
| Shear modulus $\left(G_{0_{B(natural)}}, G_{0_{B(LDPE)}}\right)$ | 3.356 x 10$^6$ Pa, 3.448 x 10$^7$ Pa |
| Poisson's ratio $\left(\nu_{0_{B(natural)}}, \nu_{0_{B(LDPE)}}\right)$ | 0.49, 0.45 |

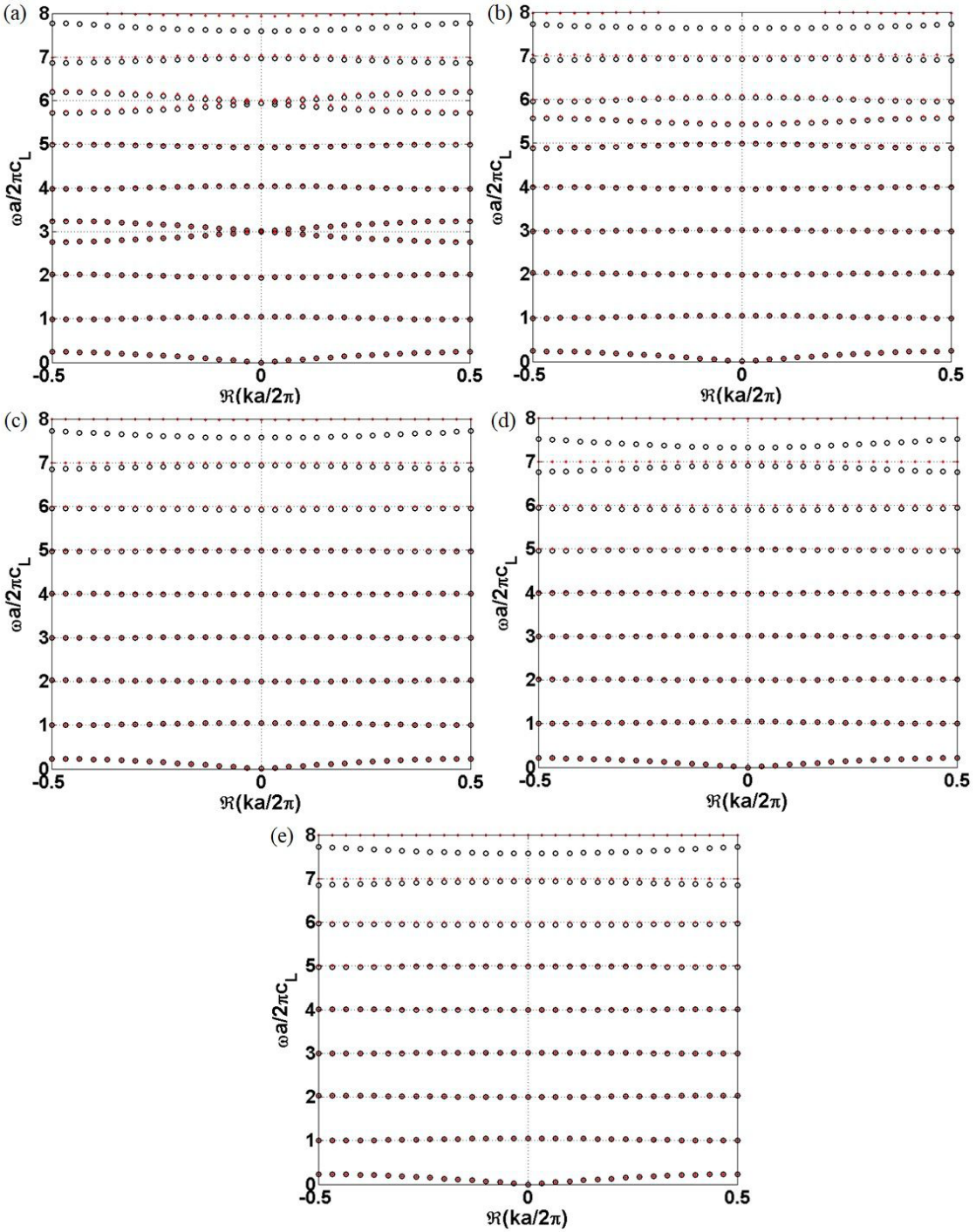


**Figure 2.** Band structure (only propagating waves) of the 1-D VPnC rod with steel inclusions in a polymeric matrix (*i.e.*, (a) epoxy, (b) nylon, (c) LDPE, (d) natural rubber, and (e) silicon rubber) without viscoelasticity computed by IPWE, considering 21 (black circles) and 42 (red points) plane waves.

A good matching between IPWE and EPWE is observed in Figure 3a. However, IPWE can only obtain the propagating modes (i.e., only real part of $\mathrm{k}$) whereas EPWE get both propagating and evanescent modes (i.e., imaginary and complex values of $\mathrm{k}$). There are only a disagreement between 3-4 and 5-6 (values of the normalized frequency, i.e., $\omega a / 2\pi c_L$), since in these ranges of frequency the waves are evanescent (with complex values of $\mathrm{k}$) and IPWE cannot obtain the information of real values of wave number with complex values. Furthermore, in Figure 3, it can be seen the formation of eight band gaps (a) and the unit cell wave attenuation ($\Im\{\mathrm{k}\}a^{12}$) associated with them (b).

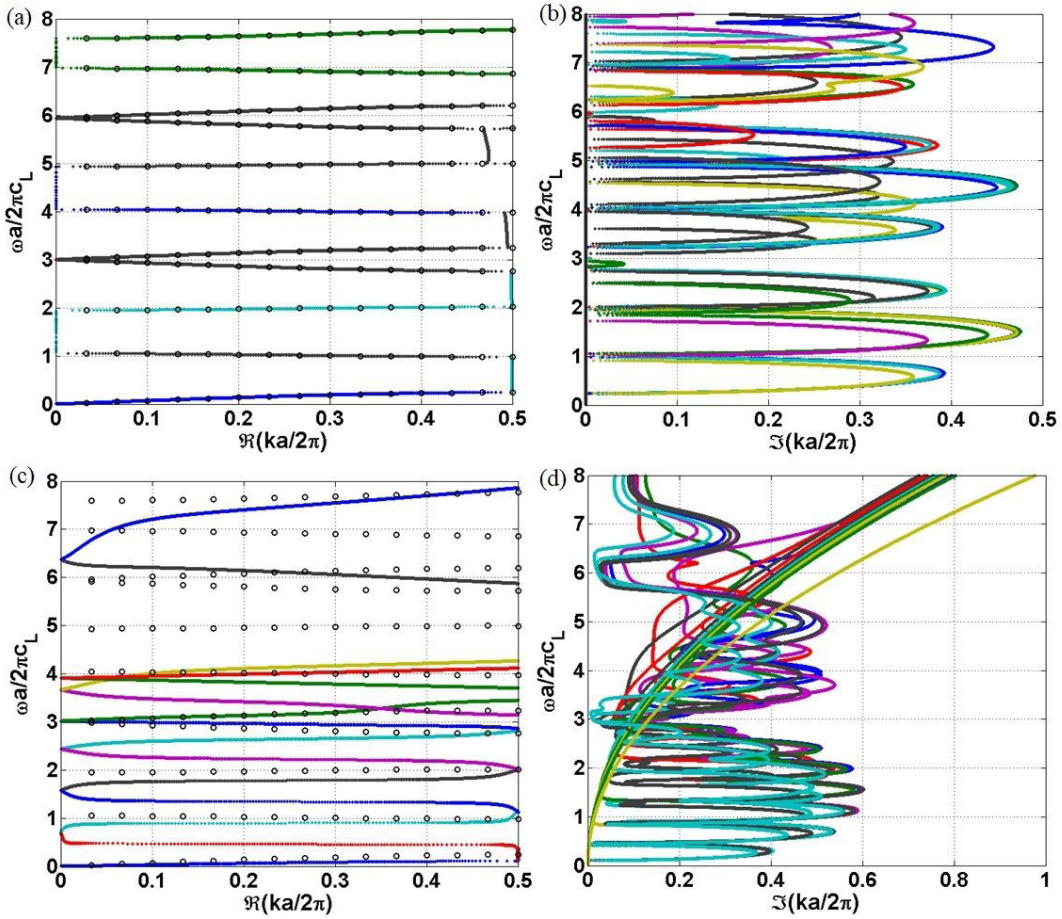


**Figure 3.** Complex band structure of the 1-D VPnC rod with steel inclusions in an epoxy matrix (a-b) without and (c-d) with viscoelasticity computed by (a, c) IPWE (black circles) and (a-d) EPWE (colored points) approaches.

In Figure 3c-d, it can be observed the complex band structure when the viscoelasticity of epoxy using SLSM is included. IPWE (black circles) cannot obtain the correct real part of wave modes (Figure 3c), since all Bloch wave modes are complex because of viscoelastic effect. It is important to highlight that all wave modes are evanescent when the viscoelasticity is considered, thus the classical definition of band gap (i.e., all wave modes must be evanescent within a complete band gap[30]) cannot be directly applied in order to identify them for VPnCs. Moreover, it can be seen in Figure 3d that there are some wave modes shifted from origin (i.e., increasing their values with the increase of frequency), which is a typical behavior of the viscoelastic periodic structures[41]. Moreover, it can also be seen in Figure 3c that sharp corners at high symmetry points (i.e., $\Re\{k\}a/2\pi = 0$ and $\Re\{k\}a/2\pi = 0.5$) become rounded[26].

Figure 4a-b illustrates the wave mode shapes of the 1-D VPnC rod at the lower ($\omega a/2\pi c_L = 0.2404$) (a) and upper ($\omega a/2\pi c_L = 0.9820$) (b) edge frequencies, considering $\Re\{k\}a/2\pi = 0.5$, of the first band gap in Figure 3a, i.e., for the epoxy matrix without viscoelasticity. These wave mode shapes in Figure 4a-b were computed by using IPWE and they present an opposite pattern, similar to the wave mode shapes of 2-D mechanical metamaterials[12]. The profiles of wave mode shapes in Figure 4a-b have a typical pattern at the edge frequencies of Bragg scattering band gaps[12].

In Figure 4c, it can be seen the wave mode shapes approximately at the middle frequency of the first "band gap" for the cases without viscoelasticity (black points), at $\omega a/2\pi c_L = 0.5802$ and $ka/2\pi = 9.4554 + 0.3585i$ of Figure 3a-b, and with viscoelasticity (red points), at $\omega a/2\pi c_L = 0.2702$ and $ka/2\pi = 9.4516 + 0.3684i$ of Figure 3c-d, considering the minimum value of $\Im\{k\}a/2\pi$. The wave mode shape patterns in Figure 4c are specific of evanescent modes, since the amplitudes decrease along the unit cell length. Moreover, the wave mode shape for the case with viscoelasticity (red points) shows higher values until -10 m (the middle of the unit cell is located at 0 m of x axis).

Figure 5 shows the complex band structure of the 1-D VPnC rod without (a-b) and with (c-d) viscoelasticity considering nylon as polymeric matrix. A good matching between IPWE (black circles) and EPWE (colored points) is observed in Figure 5a. There are disagreements between 5.6-6 and 7-7.6 (values of the normalized frequency), since in these ranges of frequency there are evanescent waves and IPWE cannot obtain their information. Furthermore, in Figure 5, it can be seen the formation of nine band gaps (a) and the unit cell wave attenuation associated with them (b).

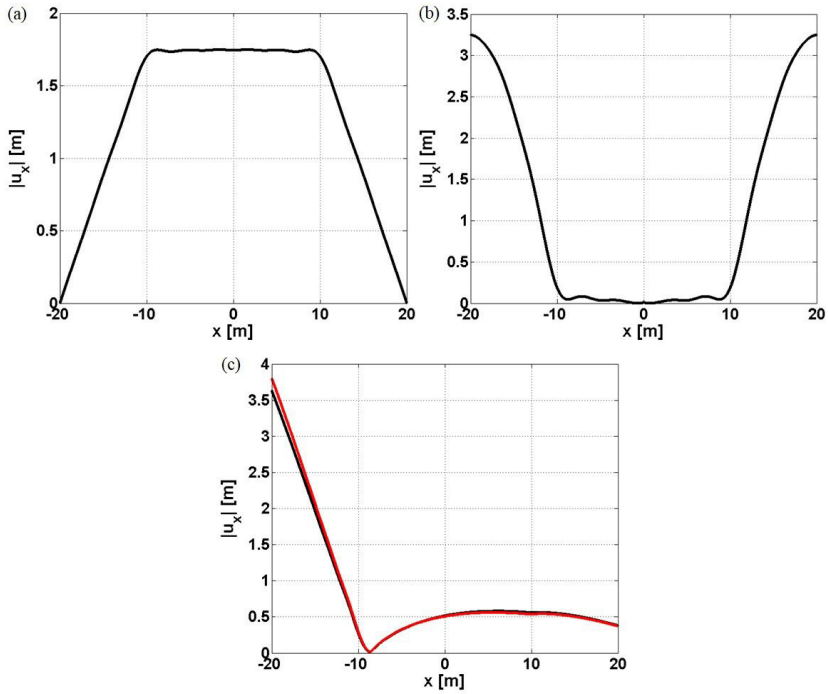


**Figure 4.** Wave mode shapes of the 1-D VPnC rod with steel inclusions in an epoxy matrix at the (a) lower and (b) upper edge frequencies of the first band gap (both computed by IPWE) and, approximately, at the (c) middle frequency of the first band gap (computed by EPWE, considering the minimum value of $\Im\{k\}a/2\pi$) without (black points) and with (red points) viscoelasticity.

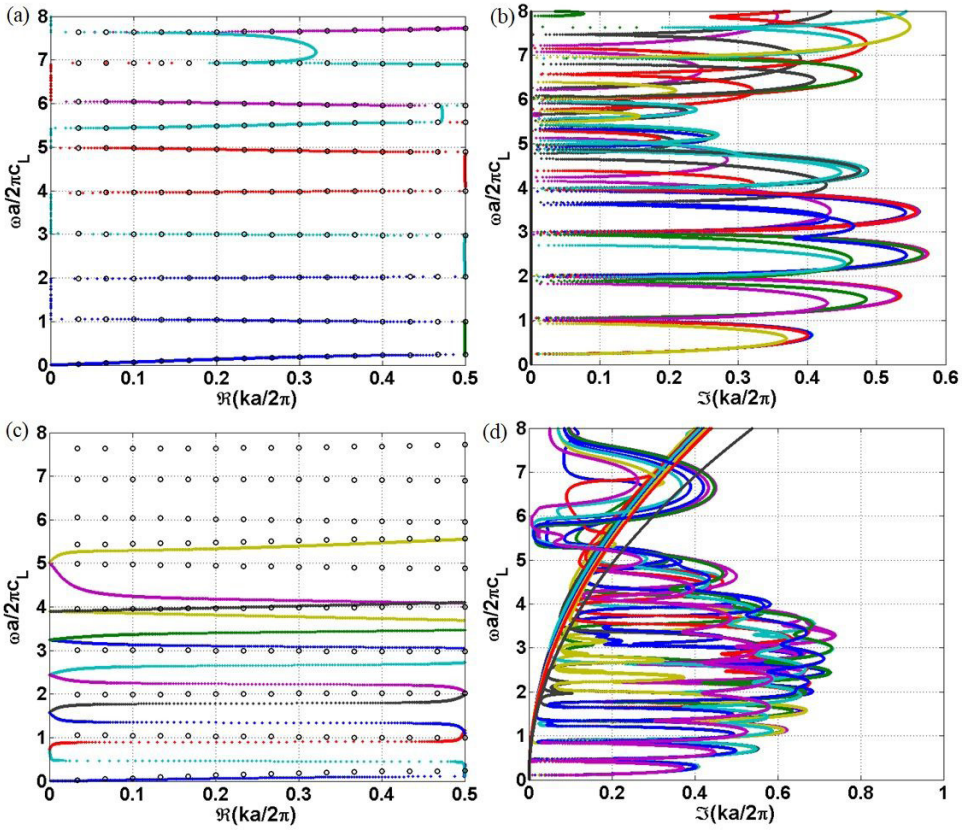


**Figure 5.** Complex band structure of the 1-D VPnC rod with steel inclusions in a nylon matrix (a-b) without and (c-d) with viscoelasticity computed by (a, c) IPWE (black circles) and (a-d) EPWE (colored points) approaches.

Figure 5c-d illustrates the complex band structure considering the viscoelastic effect of nylon. Similar as Figure 3, in Figure 5, IPWE (black circles in Figures 3c and 5c) cannot obtain the correct real part of wave modes because all Bloch wave modes are complex and wave modes are shifted from origin (in Figure 5d).

In Figure 6, it is reported the complex band structure of the 1-D VPnC rod without (a-b) and with (c-d) viscoelastic effect considering LDPE as polymeric matrix. A good agreement between IPWE (black circles) and EPWE (colored points) is seen in Figure 6a. Moreover, for this polymeric matrix (LDPE), there are no disagreements until $\omega a / 2\pi c_L = 8$, considering the positive values of k (Figure 6a). In addition, it seems that some of the branches in Figure 6a are flat bands (i.e., zero group velocity), which is a typical behavior of energy localization[11]. However, by analyzing the wave mode shapes (not shown here for brevity) of these branches it can be confirmed that they do not have the profile of typical flat bands, which is in accordance with Dal Poggetto et al.[11] (i.e., flat bands appear only for the case of hard matrix with soft inclusion). Moreover, it should be highlighted that EPWE cannot easily obtain the flat bands, since the identification of these bands with this approach (i.e., $k(\omega)$) depends on the spectral discretization ($\Delta\omega$)[11]. In Figure 6, it can be seen also the formation of eight band gaps (a) and the unit cell wave attenuation associated with them (b). Note that the unit cell wave attenuation increases with frequency (Figure 6b) for this case (LDPE matrix).

In Figure 6c-d, it is illustrated the complex band structure considering the viscoelastic effect of LDPE. Similar as explained for previous cases, IPWE (black circles) cannot obtain the correct real part of wave modes because all wave modes are complex and wave modes are shifted from origin. For this case (LDPE matrix), the imaginary part of evanescent modes (Figure 6d) seems to be lower shifted from origin than for other matrices, i.e., epoxy (Figure 3d) and nylon (Figure 5d).

Figure 7 shows the complex band structure of the 1-D VPnC rod without (a-b) and with (c-d) viscoelastic effect considering natural rubber as polymeric matrix. A good agreement between IPWE (black circles) and EPWE (coloured points) is seen in Figure 7a, with no disagreements in this range of frequency, considering the positive values of k. In addition, it can be observed in Figure 7 the formation of eight band gaps (a) and the unit cell wave attenuation associated with them (b). The unit cell wave attenuation increases with frequency (Figure 7b) for this case (natural rubber matrix).

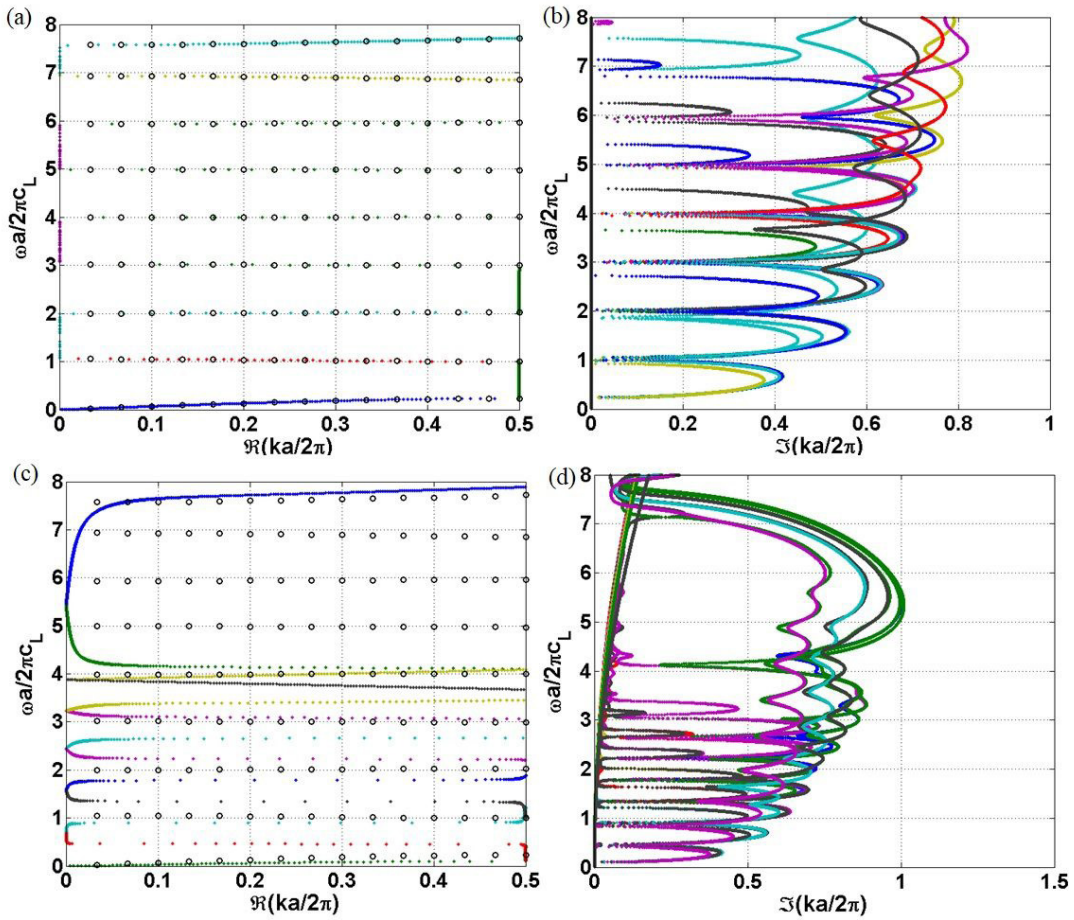


**Figure 6.** Complex band structure of the 1-D VPnC rod with steel inclusions in a LDPE matrix (a-b) without and (c-d) with viscoelasticity computed by (a, c) IPWE (black circles) and (a-d) EPWE (colored points) approaches.

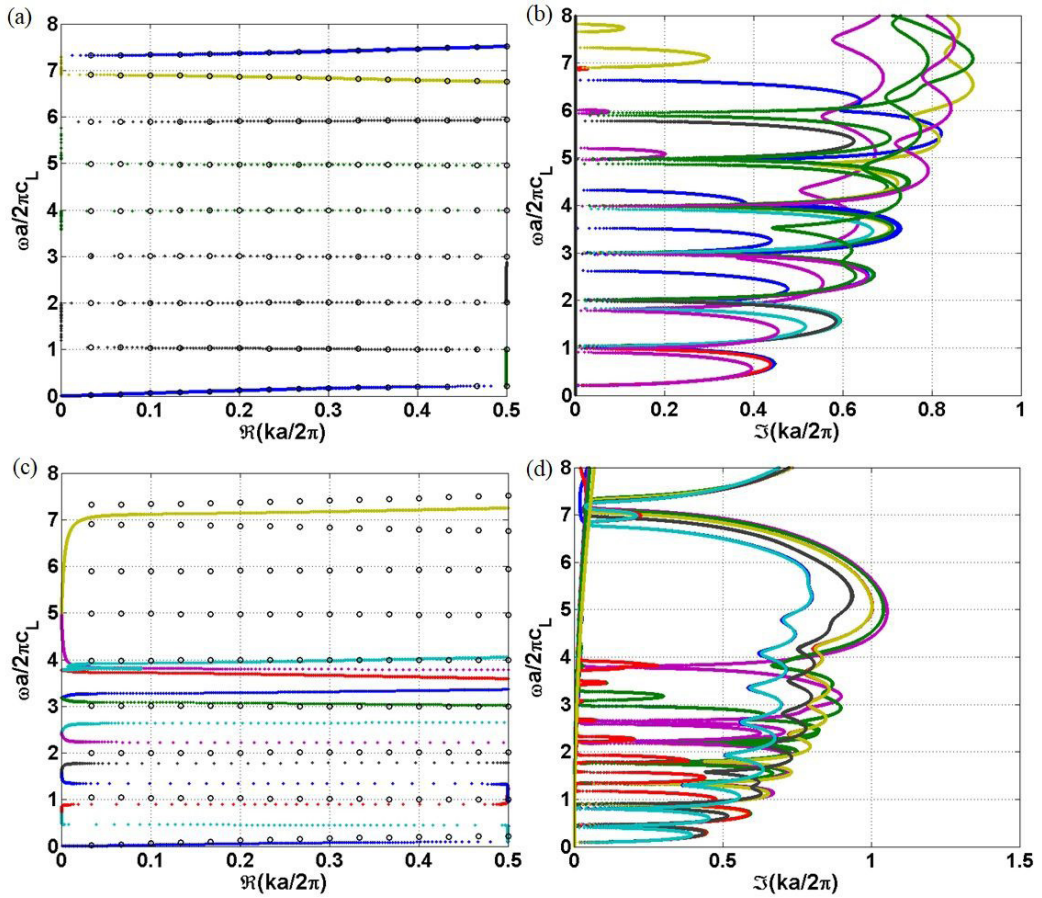


**Figure 7.** Complex band structure of the 1-D VPnC rod with steel inclusions in a natural rubber matrix (a-b) without and (c-d) with viscoelasticity computed by (a, c) IPWE (black circles) and (a-d) EPWE (colored points) approaches.

Figure 7 c-d illustrates the complex band structure considering the viscoelasticity of natural rubber. Similar to the case of LDPE (Figure 6), IPWE (black circles) cannot obtain the correct real part of wave modes because all wave modes are complex (c), wave modes are shifted from origin (d), and the imaginary part of evanescent modes seems to be lower shifted from origin than for other matrices (d), i.e., epoxy (Figure 3d), nylon (Figure 5d), and LDPE (Figure 6d).

In Figure 8, it is shown the complex band structure of the 1-D VPnC rod without (a-b) and with (c-d) viscoelastic effect considering silicon rubber as polymeric matrix. The main conclusions observed from Figure 7 (natural rubber) can also be extended for this matrix (i.e., silicon rubber) in Figure 8, since the properties of natural rubber and silicon rubber are similar (see Table 1).

Figure 9 illustrates the imaginary part of wave number (only the least attenuated wave mode, which is the second wave mode obtained by the EPWE) of the 1-D VPnC rod without (a) and with (b) viscoelastic effect. It should be highlighted that wave modes corresponding to the branch with the smallest imaginary part of k (least attenuated waves) contribute the most to the evanescent behavior[11,42]. It can be observed for both cases, i.e., without (a) and with (b) viscoelasticity, that there are two typical behaviors, one for epoxy (blue) and nylon (green), and the other for LDPE (red), silicone rubber (brown), and natural rubber (black). The unit cell wave attenuations ($\Im\{k\}a$) are higher for natural rubber, silicone rubber, and LDPE, respectively, considering the most range of frequency, with a peak value ($\Im\{k\}a/2\pi$) of 1.048 near $\omega a/2\pi c_L = 5.52$ for silicone rubber with viscoelasticity (Figure 9b). Epoxy and nylon matrices present the lower wave attenuations, respectively. However, for the range of frequency between, approximately, $4 \le \omega a/2\pi c_L \le 6$, epoxy shows a higher wave attenuation than nylon.

To understand the effect of viscoelasticity for each polymeric matrix, it is presented in Figure 10 the least attenuated wave mode (which is the second wave mode in most cases obtained by the EPWE) of the 1-D VPnC rod without (blue) and with (red) viscoelastic effect for each polymer, i.e., epoxy (a), nylon (b), LDPE (c), natural rubber (d), and silicone rubber (e). The viscoelasticity increases the unit cell wave attenuation for most range of frequency for all cases (a-e). However, there are some spectral regions for each matrix where the attenuation is higher without considering viscoelastic effect, such as $4.17 \le \omega a/2\pi c_L \le 4.65$ and $6.95 \le \omega a/2\pi c_L \le 7.73$ (for epoxy in (a)), $2.75 \le \omega a/2\pi c_L \le 3.59$ and $4.29 \le \omega a/2\pi c_L \le 4.83$ (for nylon in (b)), $7.42 \le \omega a/2\pi c_L \le 8$ (for LDPE in (c)), $6.66 \le \omega a/2\pi c_L \le 7.75$ (for natural rubber in (d)), and $7.49 \le \omega a/2\pi c_L \le 8$ (for silicone rubber in (e)).

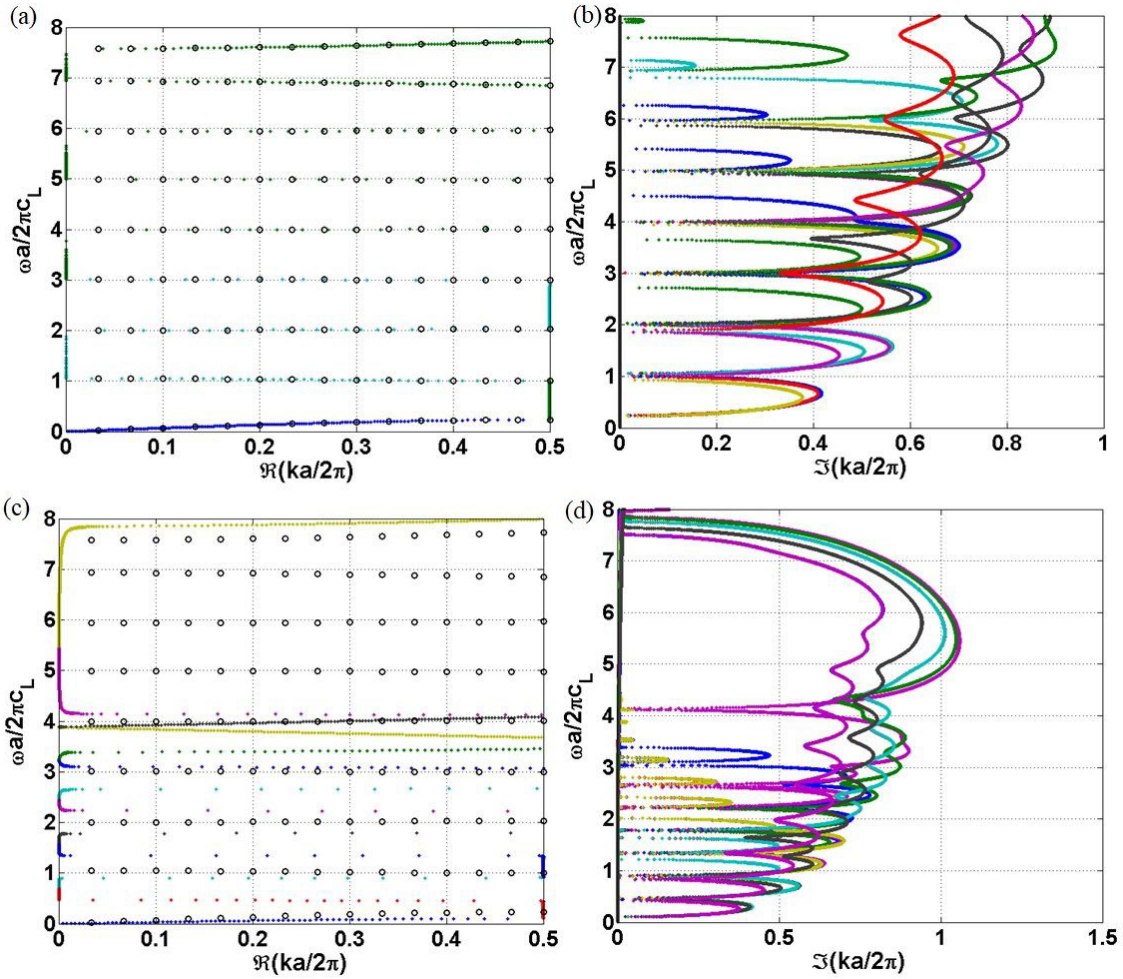


**Figure 8.** Complex band structure of the 1-D VPnC rod with steel inclusions in a silicon rubber matrix (a-b) without and (c-d) with viscoelasticity computed by (a, c) IPWE (black circles) and (a-d) EPWE (colored points) approaches.

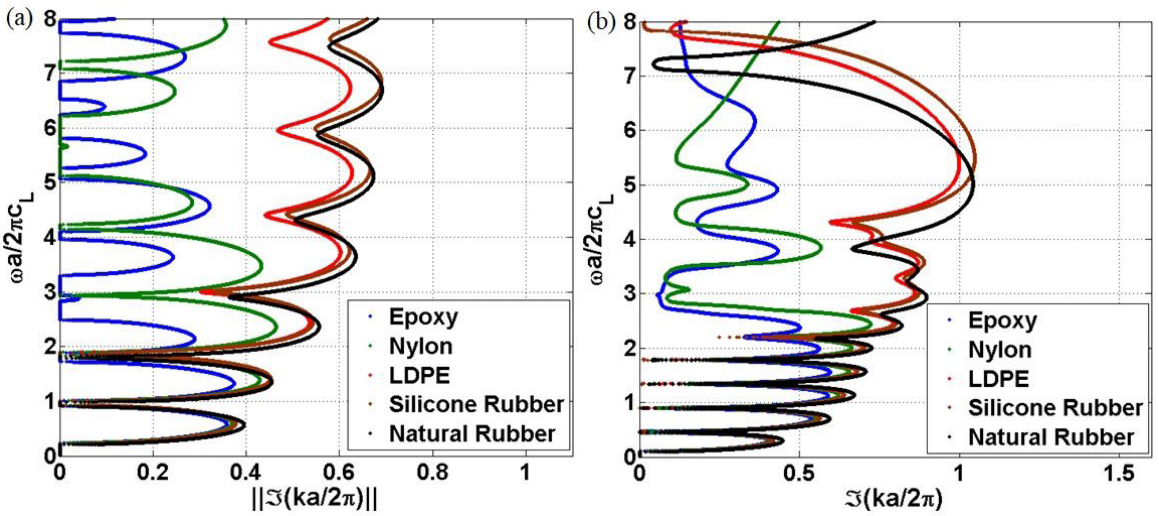


**Figure 9.** Imaginary part of the complex band structures (only the second mode is shown) of the 1-D VPnC rod with steel inclusions in different polymeric (*i.e.*, epoxy in blue, nylon in green, LDPE in red, silicon rubber in brown, and natural rubber in black) matrices (a) without and (b) with viscoelasticity computed by EPWE.

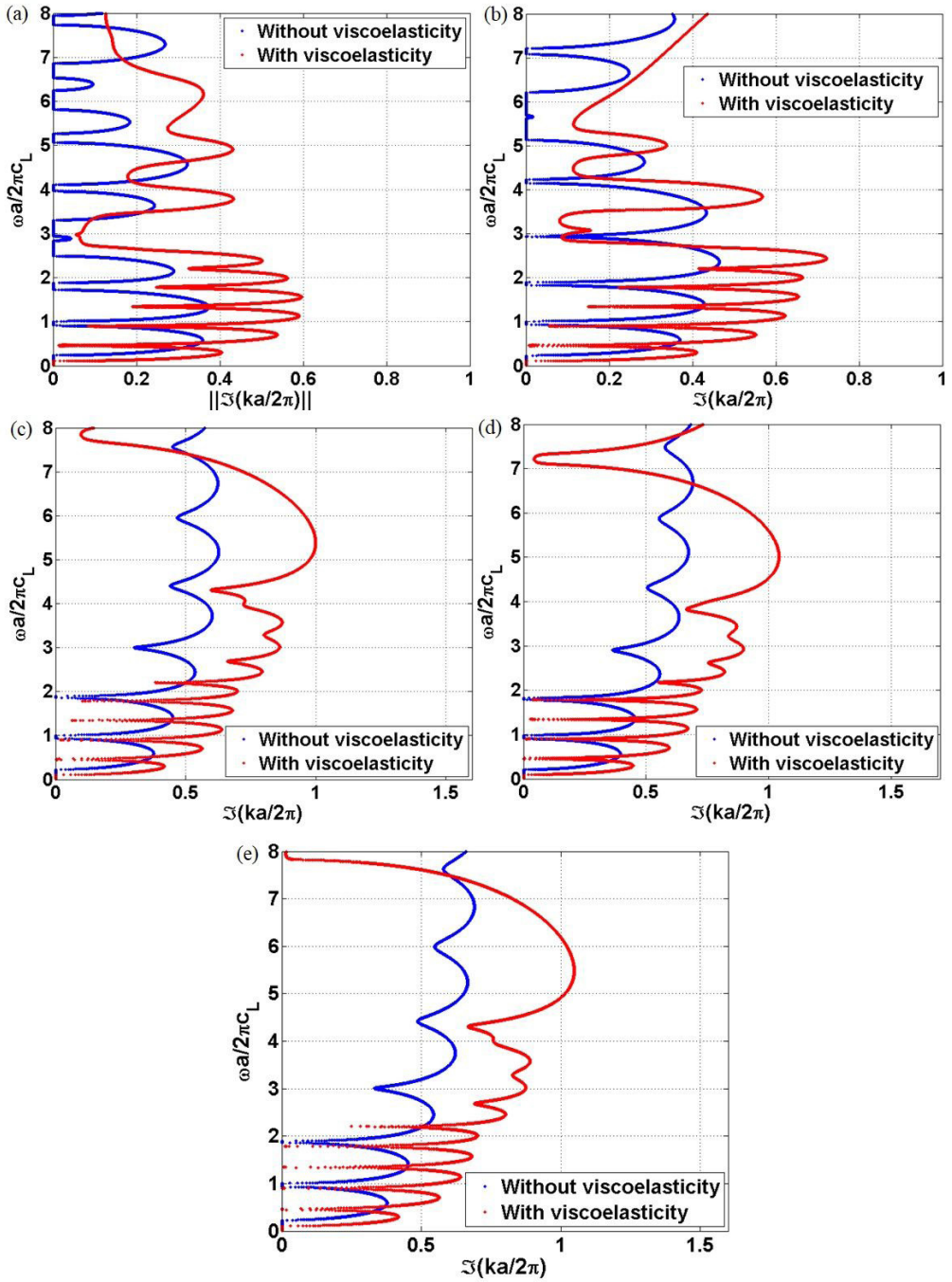


**Figure 10.** Imaginary part of the complex band structures (only the second mode is shown in most cases) of the 1-D VPnC rod with steel inclusions in an (a) epoxy, (b) nylon, (c) LDPE, (d) natural rubber, and (e) silicon rubber matrices without (blue) and with (red) viscoelasticity computed by EPWE.

## 4. Conclusion

The complex band structure of longitudinal waves in 1-D VPnC rods composed by steel inclusions (elastic material) in different polymeric matrices (i.e., epoxy, nylon, silicon rubber, natural rubber, and LDPE) with viscoelasticity (modelled by SLSM) is obtained by using the IPWE and EPWE methods. The viscoelasticity increases the unit cell wave attenuation for most range of frequency considering all polymeric matrices. The higher unit wave attenuations are for natural rubber, silicone rubber, and LDPE, respectively, considering the most range of frequency, with a peak value ($\Im\{k\}a/2\pi$) of 1.048 near $\omega a/2\pi c_L = 5.52$ for silicone rubber. Moreover, epoxy and nylon matrices present lower wave attenuations, respectively. Finally, it is evident that the viscoelastic effect cannot be neglected in the study of periodic structures with polymers in order to improve the understanding of the correct behavior of elastic wave attenuation.

## 5. Acknowledgments

The authors thank the Federal Institute of Maranhão (IFMA), Brazilian funding agencies CAPES (Finance Code 001), CNPq (Grant Reference Numbers 313620/2018, 151311/2020-0, 403234/2021-2, 405638/2022-1, and 300166/2022-2), FAPEMA (Grant Reference Numbers 07168/22 and 09683/22), and FAPESP (Grant Reference Number 2018/15894-0).

## 6. References

1. Florez O, Arregui G, Albrechtsen M, Ng RC, Gomis-Bresco J, Stobbe S, et al. Engineering nanoscale hypersonic phonon transport. Nat Nanotechnol. 2022;17(9):947-51.
2. Ribeiro LHMS, Dal Poggetto VF, Arruda JRF. Robust optimization of attenuation bands of three-dimensional periodic frame structures. Acta Mech. 2022;233(2):455-75.
3. Sampaio LYM, Cerântola PCM, De Oliveira LPR. Lightweight decorated membranes as an aesthetic solution for sound insulation panels. J Sound Vibrat. 2022;532:116971.
4. Zhou Z, Fan L. A low-frequency multiple-band sound insulator without blocking ventilation along a pipe. Sci Rep. 2022;12(1):19034.
5. Rosa MIN, Pal RK, Arruda JRF, Ruzzene M. Edge states and topological pumping in spatially modulated elastic lattices. Phys Rev Lett. 2019;123(3):034301.
6. Zhang Z, Gao P, Liu W, Yue Z, Cheng Y, Liu X, et al. Structured sonic tube with carbon nanotube like topological edge state. Nat Commun. 2022;13(1):5096.
7. Wen Z, Wang W, Khelif A, Djafari-Rouhani B, Jin Y. A perspective on elastic metastructures for energy harvesting. Appl Phys Lett. 2022;120(2):020501.
8. Jiang S, Liu X, Liu J, Ye D, Duan Y, Li K, et al. Flexible metamaterial electronics. Adv Mater. 2022;34(52):2200070.
9. Miranda EJP Jr, Dos Santos JMC. Band structure in carbon nanostructure phononic crystals. Mater Res. 2017; 20(Suppl. 2):555-71.
10. Miranda EJP Jr, Santos JMC. Wave attenuation in 1-3 phononic structures with lead-free piezoelectric ceramic inclusions. Physica B Condens Matter. 2022;631:413642.
11. Dal Poggetto VF, Miranda EJP Jr, Santos JMC, Pugno NM. Wave attenuation in viscoelastic hierarchical plates. Int J Mech Sci. 2022;236:107763.
12. Miranda EJP Jr, Nobrega ED, Rodrigues SF, Aranas C Jr, Dos Santos JMC. Wave attenuation in elastic metamaterial thick plates: analytical, numerical and experimental investigations. Int J Solids Struct. 2020;204-205:138-52.
13. Liu Y, Shi D, He H, Liu S, Fan H. Double-resonator based metaconcrete composite slabs and vibration attenuation mechanism. Eng Struct. 2022;262:114392.
14. Goto AM, Nóbrega ED, Pereira FN, Dos Santos JMC. Numerical and experimental investigation of phononic crystals via wave-based higher-order rod models. Int J Mech Sci. 2020;181:105776.
15. Li J, Yang P, Ma Q, Xia M. Complex band structure and attenuation performance of a viscoelastic phononic crystal with finite out-of-plane extension. Acta Mech. 2021;232(8):2933-54.
16. Vakilifard M, Mahmoodi MJ. Evanescent waves attenuation and stiffness enhancement of viscoelastic locally resonant metamaterials by nanofiller addition- a multi-scale k(ω) based modeling. Mech Mater. 2021;160:103969.
17. Zhang S, Wang Y, Wang Y. Evanescent surface acoustic waves in 1D viscoelastic phononic crystals. J Appl Phys. 2021;129(24):245111.
18. Wang T, Laude V, Kadic M, Wang IF, Wang IS. Complex-eigenfrequency band structure of viscoelastic phononic crystals. Appl Sci (Basel). 2019;9(14):2825.
19. Chen Y, Guo D, Li YF, Li G, Huang X. Maximizing wave attenuation in viscoelastic phononic crystals by topology optimization. Ultrasonics. 2019;94:419-29.
20. Lou J, He L, Yang J, Kitipornchai S, Wu H. Wave propagation in viscoelastic phononic crystal rods with internal resonators. Appl Acoust. 2018;141:382-92.
21. Mukhopadhyay T, Adhikari S, Batou A. Frequency domain homogenization for the viscoelastic properties of spatially correlated quasi-periodic lattices. Int J Mech Sci. 2019;150:784-806.
22. Lewińska MA, Kouznetsova VG, van Dommelen JAW, Krushynska AO, Geers MGD. The attenuation performance of locally resonant acoustic metamaterials based on generalised viscoelastic modelling. Int J Solids Struct. 2017;126-127:163-74.
23. Lakes R. Viscoelastic materials. New York: University Press; 2009.
24. Lin C. Rethinking and researching the physical meaning of the standard linear solid model in viscoelasticity. Mech Adv Mater Structures. 2023. In press.
25. Miranda EJP Jr, Rodrigues SF, Dos Santos JMC. Complex dispersion diagram and evanescent modes in piezomagnetic phononic structures. Solid State Commun. 2022;346:114697.
26. Schalcher LFC, Santos JMC, Miranda EJP Jr. Extended plane wave expansion formulation for 1-D viscoelastic phononic crystals. Partial Differential Equations in Applied Mathematics. 2023;7:100489.
27. Li L. Use of Fourier series in the analysis of discontinuous periodic structures. J Opt Soc Am A Opt Image Sci Vis. 1996;13(9):1870-6.
28. Cao Y, Hou Z, Liu Y. Convergence problem of plane-wave expansion method for phononic crystals. Phys Lett A. 2004;327(2-3):247-53.
29. Hsue Y-C, Yang T-J. Contour of the attenuated length of an evanescent wave at constant frequency within a band gap of photonic crystal. Solid State Commun. 2004;129(7):475-8.
30. Laude V, Achaoui Y, Benchabane S, Khelif A. Evanescent Bloch waves and the complex band structure of phononic crystals. Phys Rev B Condens Matter Mater Phys. 2009;80(9):092301.
31. Brillouin L. Wave propagation in periodic structures. New York/USA: Dover Publications, 1946.
32. Assis GFCA, Beli D, Miranda EJP Jr, Camino JF, Santos JMC, Arruda JRF. Computing the complex wave and dynamic behavior of one-dimensional phononic systems using a state-space formulation. Int J Mech Sci. 2019;163:105088.
33. Lee D, Kim M, Rho J. A finite element method towards acoustic phononic crystals by weak formulation. J Phys Condens Matter. 2019;31(37):375901.
34. Kim SA, Johnson WL. Elastic constants and internal friction of martensitic steel, ferritic-pearlitic steel, and α-iron. Mater Sci Eng A. 2007;452-453:633-9.
35. Zhao YP, Wei PJ. The band gap of 1D viscoelastic phononic crystal. Comput Mater Sci. 2009;46(3):603-6.
36. Wei PJ, Zhao YP. The influence of viscosity on band gaps of 2D phononic crystal. Mech Adv Mater Structures. 2010;17(6):383-92.
37. Kettenbeil C, Ravichandran G. Experimental investigation of the dynamic behavior of metaconcrete. Int J Impact Eng. 2018;111:199-207.
38. Mitchell SJ, Pandolfi A, Ortiz M. Metaconcrete: designed aggregates to enhance dynamic performance. J Mech Phys Solids. 2014;65(1):69-81.
39. Callister WD, Rethwisch DG. Materials science and engineering: an introduction. Hoboken: John Wiley; 2009.
40. Mencik J. On the low- and mid-frequency forced response of elastic structures using wave finite elements with one-dimensional propagation. Comput Struc. 2010;88(11-12):674-89.
41. Moiseyenko RP, Laude V. Material loss influence on the complex band structure and group velocity in phononic crystals. Physica B Condens Matter. 2011;83(6):064301.
42. Xiao Y, Wen J, Wen X. Broadband locally resonant beams containing multiple periodic arrays of attached resonators. Phys Lett A. 2012;376(16):1384-90.